Measurement of the Inclusive Jet Cross Section using the k_T algorithm in $p\overline{p}$ Collisions at $\sqrt{s} = 1.96$ TeV

(CDF Collaboration)

PRD Draft v0.0

(May 2nd 2006)

We report on new measurements of the inclusive jet production cross section as a function of the jet transverse momentum in $p\overline{p}$ collisions at $\sqrt{s} = 1.96$ TeV using data collected with the upgraded Collider Detector at Fermilab in Run II, corresponding to an integrated luminosity of 0.98 fb^{-1}. The measurements are carried out in five different jet rapidity regions for jets with $|y^{jet}| < 2.1$ and transverse momentum in the range $54 < p_T^{jet} < 700$ GeV/c. Next-to-leading order perturbative QCD predictions are in good agreement with the measured cross sections after the necessary non-perturbative parton-to-hadron corrections are included.

PACS numbers: PACS numbers 12.38.Aw, 13.85.-t, 13.87.-a

I. INTRODUCTION

The measurement of the inclusive jet cross section as a function of the jet transverse momentum, p_T^{jet}, in $p\overline{p}$ collisions at $\sqrt{s} = 1.96$ TeV constitutes a test of perturbative QCD (pQCD) [1] predictions over more than eight orders of magnitude in cross section and probes distances down to 10^{-19}m. The increased center-of-mass energy and integrated luminosity in Run II at the Tevatron have allowed to measure the jet cross section for jets with transverse momentum up to about 700 GeV/c [2, 3], thus extending the p_T^{jet} range by more than 150 GeV/c compared to Run I [4, 5]. In particular, the CDF experiment recently published results [2] on inclusive jet production using the k_T algorithm [6, 7] for jets with $p_T^{jet} > 54$ GeV/c and rapidity [8] in the region $0.1 < |y^{jet}| < 0.7$, which are well described by NLO pQCD predictions [9]. The pQCD calculations are written as matrix elements, describing the hard interaction between partons, convoluted with parton density functions (PDFs) [10, 11] in the proton and antiproton that require input from the experiments. Inclusive jet cross section measurements from Run I at the Tevatron [5], performed in

different jet rapidity regions, have been used to partially constrain the gluon distribution in the proton. As noted in [2], the pQCD predictions are affected by the still limited knowledge of the gluon PDF, which translates into a big uncertainty on the theoretical cross sections at high p_T^{jet}. This article presents new measurements of the inclusive jet production cross section as a function of p_T^{jet} in five different jet rapidity regions up to $|y^{jet}| = 2.1$, using the k_T algorithm and based on 0.98 fb^{-1} of CDF Run II data. The measurements are corrected to the hadron level [12] and compared to pQCD NLO predictions.

II. EXPERIMENTAL SETUP

The CDF II detector (see Figure 1) is described in detail in [13]. Here, the sub-detectors most relevant for this analysis are briefly discussed. The detector has a charged particle tracking system immersed in a 1.4 T magnetic field, aligned coaxially with the beam line. A silicon microstrip detector [14] provides tracking over the radial range 1.35 to 28 cm and covers the pseudorapidity range $|\eta| \leq 2$. A 3.1 m long open-cell drift chamber, the Central Outer Tracker (COT) [15], covers the radial range from 44 to 132 cm and provides tracking coverage for $|\eta| \leq 1$. Segmented sampling calorimeters, arranged in a projective tower geometry, surround the tracking system and measure the energy flow of interacting particles in $|\eta| \leq 3.6$. The CDF central barrel calorimeter [16] is unchanged from Run I and covers the region $|\eta| < 1$. It consists of an electromagnetic calorimeter (CEM) and an hadronic calorimeter (CHA) segmented into 480 towers of size 0.1 in η and 15° in ϕ. The end-wall hadronic calorimeter (WHA) [17] complements the coverage of the central barrel calorimeter in the region $0.6 < |\eta| < 1.0$ and provides additional forward coverage out to $|\eta| < 1.3$. In Run II, new forward scintillator-plate calorimeters [18] replaced the original Run I gas calorimeter system. The new plug electromagnetic calorimeter (PEM) covers the region $1.1 < |\eta| < 3.6$ while the new hadronic calorimeter (PHA) provides coverage in the $1.3 < |\eta| < 3.6$ region. The calorimetry has a crack at $\eta = 0$ (between the two halves of the central barrel calorimeter) and two cracks at $\eta = \pm 1.1$ (in the region between the WHA and the plug calorimeters). The measured energy resolutions for electrons in the electromagnetic calorimeters are $14\%/\sqrt{E_T}$ (CEM) and $16\%/\sqrt{E} \oplus 1\%$ (PEM) where the energies are expressed in GeV. The single-pion energy resolutions in the hadronic calorimeters, as determined in test-beam data, are $75\%/\sqrt{E_T}$ (CHA), $80\%/\sqrt{E}$ (WHA) and $80\%/\sqrt{E} \oplus 5\%$ (PHA). Cherenkov counters located in the $3.7 < |\eta| < 4.7$ region [19] measure the average number of inelastic $p\overline{p}$ collisions per bunch crossing and thereby determine the beam luminosity.

III. JET RECONSTRUCTION

The k_T algorithm is used to reconstruct jets in data and Monte Carlo simulated events (see Section VI) from the energy depositions in the calorimeter towers with transverse momentum above 0.1 GeV/c. First, all towers are considered as protojets. The quantities

$$k_{T,i} = p^2_{T,i} \quad ; \quad k_{T,(i,j)} = \min(p^2_{T,i}, p^2_{T,j}) \cdot \Delta R^2_{i,j}/D^2, \tag{1}$$

are computed for each protojet and pair of protojets respectively, where $p_{T,i}$ denotes the transverse momentum of the ith protojet, $\Delta R_{i,j}$ is the distance ($y - \phi$ space) between each pair of protojets, and D is a parameter that approximately controls the size of the jet. All $k_{T,i}$ and $k_{T,(i,j)}$ values are then collected into a single sorted list. In this combined sorted list, if the smallest quantity is of the type $k_{T,i}$, the corresponding protojet is promoted to be a jet and removed from the list. Otherwise, if the smallest quantity is of the type $k_{T,(i,j)}$, the protojets are combined into a single protojet by summing up their four-vector components. The procedure is iterated over protojets until the list is empty. The jet transverse momentum, rapidity, and azimuthal angle are denoted as $p^{jet}_{T,CAL}$, y^{jet}_{CAL}, and ϕ^{jet}_{CAL}, respectively. The same jet algorithm is applied to the final-state particles in the Monte Carlo event samples to search for jets at the hadron level. In this case, no cut on the minimum transverse momentum of the particles is applied. The resulting hadron-level jet variables are denoted as $p^{jet}_{T,HAD}$, y^{jet}_{HAD}, and ϕ^{jet}_{HAD}.

IV. EVENT SELECTION

The measurements presented in this article correspond to a total integrated luminosity of 0.98 ± 0.06 fb^{-1} of data collected by the CDF experiment in Run II. Events were selected *online* using three-level trigger paths [20], based on the measured energy deposits in the calorimeter towers, with several different thresholds on the jet transverse energies and different prescales (see Table I). In the first-level trigger, a single trigger tower with transverse energy above 5 GeV or 10 GeV, depending on the trigger path, is required. In the second-level trigger, a hardware-based clustering is carried out where calorimeter clusters are formed around the selected trigger towers. The events are required to have at least one second-level trigger cluster with transverse energy above a given threshold, which varies between 15 and 90 GeV for the different trigger paths. In the third-level trigger, jets are reconstructed using the CDF Run I cone algorithm [21] and the events are required to have at least one jet with transverse energy above 20 to 100 GeV

depending on the trigger path.

Trigger Path	Level 1 tower E_T [GeV]	Level 2 cluster E_T [GeV]	Level 3 jet E_T [GeV]	eff. prescale
Jet 20	5	15	20	777.0
Jet 50	5	40	50	34.3
Jet 70	10	60	70	8.0
Jet 100	10	90	100	1.0

TABLE I: Summary of trigger paths, trigger thresholds and effective prescales employed to collect the data.

Jets are then searched for using the k_T algorithm, as explained above, with $D = 0.7$. For each trigger data sample, the threshold on the minimum $p_{T,CAL}^{jet}$ is chosen in such a way that the trigger selection is fully efficient. The following selection criteria has been imposed:

- The events are selected to have at least one reconstructed primary vertex with z-position within 60 cm around the nominal interaction point.
- Events are required to have at least one jet with rapidity in the region $|y_{CAL}^{jet}| < 2.1$ and corrected transverse momentum (see below) above 54 GeV/c.
- In order to remove beam-related backgrounds and cosmics rays, the events are required to fulfill $\not{E}_T/\sqrt{\Sigma E_T} < F(p_{T,CAL}^{leading\ jet})$, where $\not{E}_T$ denotes the missing transverse energy [22] and $\Sigma E_T = \sum_i E_T^i$ is the total transverse energy of the event, as measured using calorimeter towers with E_T^i above 0.1 GeV. The threshold function $F(p_{T,CAL}^{leading\ jet})$ is defined as $F(p_T^{jet}) = \min(2 + 0.0125 \times p_T^{jet}, 7)$, where $p_{T,CAL}^{leading\ jet}$ is the uncorrected transverse momentum of the leading jet (highest p_T^{jet}) and the units are GeV. This criterion is designed to preserve more than 95% of the QCD events, as determined from Monte Carlo studies. A visual scan for $p_{T,CAL}^{jet} > 400$ GeV/c showed no remaining backgrounds.

Measurements are carried out in five different y_{CAL}^{jet} regions: $|y_{CAL}^{jet}| < 0.1$, $0.1 < |y_{CAL}^{jet}| < 0.7$, $0.7 < |y_{CAL}^{jet}| < 1.1$, $1.1 < |y_{CAL}^{jet}| < 1.6$, and $1.6 < |y_{CAL}^{jet}| < 2.1$, where the different thresholds are dictated by the layout of the CDF calorimeter system. The measurements are limited to jets with $|y_{CAL}^{jet}| < 2.1$ to avoid contributions from the proton/antiproton remnants that would affect the measured $p_{T,CAL}^{jet}$ in the most forward region of the calorimeter.

V. EFFECT OF MULTIPLE $P\overline{P}$ INTERACTIONS

The measured jet transverse momentum includes additional contributions from multiple proton-antiproton interactions per bunch crossing at high instantaneous luminosity. The data used in this measurement were collected

at Tevatron instantaneous luminosities between $0.2 \times 10^{31}\mathrm{cm}^{-2}\mathrm{s}^{-1}$ and $16.3 \times 10^{31}\mathrm{cm}^{-2}\mathrm{s}^{-1}$ with an average of $4.1 \times 10^{31}\mathrm{cm}^{-2}\mathrm{s}^{-1}$, for which, in average, 1.5 inelastic proton-antiproton interactions per bunch crossing are expected. At the highest instantaneous luminosities considered, an average of 5.9 interactions per bunch crossing are produced. This mainly affects the measured cross section at low $\mathrm{p}_{\mathrm{T}}^{\mathrm{jet}}$ where the contributions are sizeable. In CDF, multiple interactions are identified via the presence of additional primary vertices reconstructed from charged particles. The measured jet transverse momenta are corrected for this effect by removing a certain amount of transverse momentum, ϵ, for each additional primary vertex, as determined from the data by requiring that, after the correction is applied, the ratio of cross sections at low and high instantaneous luminosities does not show any $\mathrm{p}_{\mathrm{T}}^{\mathrm{jet}}$ dependence. The study is carried out separately in each $\mathrm{y}_{\mathrm{CAL}}^{\mathrm{jet}}$ region, and the results are consistent with a common value $\epsilon = 1.62^{+0.70}_{-0.46}$ GeV/c across the whole rapidity range. The quoted uncertainties on ϵ include both statistical and systematic contributions, the latter are related to the precise definition of low and high instantaneous luminosity samples.

VI. MONTE CARLO SIMULATION

Monte Carlo event samples are used to determine the response of the detector and the correction factors to the hadron level. The generated samples are passed through a full CDF detector simulation (based on GEANT3 [23] where the GFLASH [24] package is used to simulate the energy deposition in the calorimeters) and then reconstructed and analyzed using the same analysis chain as in the data. Samples of simulated inclusive jet events have been generated using PYTHIA 6.203 [25] and HERWIG 6.4 [26] Monte Carlo generators. CTEQ5L [27] parton distribution functions are used for the proton and antiproton. The PYTHIA samples have been created using a special tuned set of parameters, denoted as PYTHIA-Tune A [28], that includes enhanced contributions from initial-state gluon radiation and secondary parton interactions between remnants. Tune A was determined as a result of dedicated studies of the underlying event using the CDF Run I data [29] and has been shown to properly describe the measured jet shapes in Run II [30]. In the case of PYTHIA, fragmentation into hadrons is carried out using the string model [31] as implemented in JETSET [32], while HERWIG implements the cluster model [33].

A. Simulation of the calorimeter response to jets

Dedicated studies have been performed to test the Monte Carlo description of the calorimeter response to jets in the different $|\mathrm{y}_{\mathrm{CAL}}^{\mathrm{jet}}|$ regions. Previous results [2] for jets with $0.1 < |\mathrm{y}_{\mathrm{CAL}}^{\mathrm{jet}}| < 0.7$ indicate that the simulation properly

reproduces both the average jet momentum and the jet momentum resolution as measured in the data. The study is repeated for the rest of y^{jet}_{CAL} regions using an exclusive dijet sample selected with the following criteria:

- Events are selected to have one and only one reconstructed primary vertex with z-position within 60 cm around the nominal interaction point.
- Events are required to have two jets with $p^{jet}_{T,CAL} > 10$ GeV/c, where one of the jets must be in the region $0.1 < |y^{jet}_{CAL}| < 0.7$.
- $\not{E}_T/\sqrt{\Sigma E_T} < F(p^{leading\ jet}_{T,CAL})$, as explained above.

First, the bisector method [34] is applied to data and Monte Carlo exclusive dijet events to test the accuracy of the simulated jet momentum resolution. The study indicates that the Monte Carlo simulation systematically underestimates the measured jet momentum resolution by 6 % and 10 % for jets in the regions $0.7 < |y^{jet}_{CAL}| < 1.1$ and $1.6 < |y^{jet}_{CAL}| < 2.1$, respectively, and with no significant $p^{jet}_{T,CAL}$ dependence. An additional smearing of the reconstructed jet transverse momenta is applied to the Monte Carlo events to account for this effect. In the region $1.1 < |y^{jet}_{CAL}| < 1.6$, the measured jet momentum resolution is overestimated by 5% in the simulation. The effect on the final result is included via slightly modified unfolding factors (see below). For jets with $|y^{jet}_{CAL}| < 0.7$, the Monte Carlo simulation properly describes the measured jet energy resolution. After corrections have been applied to the Monte Carlo events, data and simulation agree within a relative uncertainty of ±8% over the whole range in $p^{jet}_{T,CAL}$ and y^{jet}_{CAL} considered.

The average jet momentum calorimeter response in the simulation is then tested comparing the $p^{jet}_{T,CAL}$ balance in data and Monte Carlo exclusive dijet events, where the jet in the region $0.1 < |y^{jet}_{CAL}| < 0.7$ acts as reference. The variable β defined as:

$$\beta = \frac{1+ < \Delta P_T >}{1- < \Delta P_T >}; \quad \Delta P_T = \frac{p^{tested\ jet}_{T,CAL} - p^{ref.\ jet}_{T,CAL}}{p^{tested\ jet}_{T,CAL} + p^{ref.\ jet}_{T,CAL}} \tag{2}$$

is computed in data and simulated events in bins of $(p^{tested\ jet}_{T,CAL} + p^{ref.\ jet}_{T,CAL})/2$, where $p^{ref.\ jet}_{T,CAL}$ denotes the transverse momentum of the jet in the region $0.1 < |y^{jet}_{CAL}| < 0.7$, and $p^{tested\ jet}_{T,CAL}$ is the transverse momentum of the jet in the y^{jet}_{CAL} region under study. If considered event-by-event, β is equivalent to $p^{tested\ jet}_{T,CAL}/p^{ref.\ jet}_{T,CAL}$. Figure 2 presents the ratios β_{DATA}/β_{MC} as a function of $p^{jet}_{T,CAL} = p^{tested\ jet}_{T,CAL}$ in the different y^{jet}_{CAL} bins. The study indicates that small corrections are required around calorimeter cracks, $|y^{jet}_{CAL}| < 0.1$ and $1.1 < |y^{jet}_{CAL}| < 1.6$, as well as in the most forward region, $1.6 < |y^{jet}_{CAL}| < 2.1$. Table II summarizes the different corrections applied to the Monte Carlo simulation. For jets with

$|y^{jet}_{CAL}| > 1.1$, the correction shows a non-linear $p^{jet}_{T,CAL}$ dependence and at very high $p^{jet}_{T,CAL}$ several parameterizations are considered (see Figure 2). The difference observed in the final results using different parameterizations is included as part of the total systematic uncertainty.

y^{jet}_{CAL} region	correction applied to $p^{jet}_{T,CAL}$ in the simulation
$\lvert y^{jet}_{CAL}\rvert < 0.1$	$1.011 \cdot p^{jet}_{T,CAL}$
$0.1 < \lvert y^{jet}_{CAL}\rvert < 0.7$	-
$0.7 < \lvert y^{jet}_{CAL}\rvert < 1.1$	-
$1.1 < \lvert y^{jet}_{CAL}\rvert < 1.6$ ($p^{jet}_{T,CAL} < 110$ GeV/c)	$1.006 \cdot p^{jet}_{T,CAL} - 0.00014 \cdot {p^{jet}_{T,CAL}}^2$
$1.1 < \lvert y^{jet}_{CAL}\rvert < 1.6$ ($p^{jet}_{T,CAL} > 110$ GeV/c)	$0.996 \cdot p^{jet}_{T,CAL} - 0.00007 \cdot {p^{jet}_{T,CAL}}^2$
$1.6 < \lvert y^{jet}_{CAL}\rvert < 2.1$ ($p^{jet}_{T,CAL} < 125$ GeV/c)	$1.001 \cdot p^{jet}_{T,CAL} - 0.00020 \cdot {p^{jet}_{T,CAL}}^2$
$1.6 < \lvert y^{jet}_{CAL}\rvert < 2.1$ ($p^{jet}_{T,CAL} > 125$ GeV/c)	$0.998 \cdot p^{jet}_{T,CAL} - 0.00010 \cdot {p^{jet}_{T,CAL}}^2$

TABLE II: Summary of the corrections applied to the reconstructed jet momenta in the Monte Carlo simulation.

VII. RECONSTRUCTION OF THE JET VARIABLES

Numbers in the discussion below will change since the numbers refer to bins in $(p^{jet}_{T,CAL} + p^{jet}_{T,HAD})/2$ *while we should quote the ones computed in* $p^{jet}_{T,CAL}$ *bins, as it was done in the PRL.*

The reconstruction of the jet variables in the calorimeter is studied using Monte Carlo event samples and matched pair of jets at the calorimeter [1] and hadron levels. These studies indicate that the angular variables of a jet are reconstructed with no significant systematic shift and with a resolution better than 0.05 units in y and ϕ at low $p^{jet}_{T,CAL}$, improving as $p^{jet}_{T,CAL}$ increases. The measured jet transverse momentum systematically underestimates that of the hadron level jet. This is mainly attributed to the non-compensating nature of the calorimeter [35]. For jets with $p^{jet}_{T,CAL}$ about 50 GeV/c, the jet transverse momentum is reconstructed with an average shift that varies between -9% and -30%, depending on the jet rapidity region, and a resolution between 10% and 16%. The jet reconstruction improves as $p^{jet}_{T,CAL}$ increases. For jets with $p^{jet}_{T,CAL}$ about 500 GeV/c, the average shift is -5% and the resolution is about 7%.

VIII. UNFOLDING

The measured $p^{jet}_{T,CAL}$ distributions in the different $|y^{jet}_{CAL}|$ regions are unfolded back to the hadron level using Monte Carlo event samples. PYTHIA-TUNE A provides a reasonable description of the different jet and underlying

[1] The Monte Carlo samples include modified response to jets as discussed in Section VI.

event quantities, and is used to determine the correction factors in the unfolding procedure. In order to avoid any bias on the correction factors due to the particular PDF set used during the generation of the Monte Carlo samples, which translates into slightly different simulated $p_{T,CAL}^{jet}$ distributions, PYTHIA-TUNE A is re-weighted until it accurately follows each of the measured $p_{T,CAL}^{jet}$ distributions.

The unfolding is carried out in two steps. First, an average correction is computed separately in each jet rapidity region using matched pairs of jets at the calorimeter and hadron levels. The correlation $< p_{T,HAD}^{jet} - p_{T,CAL}^{jet} >$ vs $< p_{T,CAL}^{jet} >$, computed in bins of $(p_{T,HAD}^{jet} + p_{T,CAL}^{jet})/2$, is used to extract correction factors which are then applied to the measured jets to obtain the corrected transverse momenta, $p_{T,COR}^{jet}$. In each jet rapidity region, a raw cross section is defined as

$$\frac{d^2\sigma}{dp_{T,COR}^{jet} dy_{CAL}^{jet}} = \frac{1}{\mathcal{L}} \frac{N_{COR}^{jet}}{\Delta p_{T,COR}^{jet}\ \Delta y_{CAL}^{jet}}, \tag{3}$$

where N_{COR}^{jet} denotes the number of jets in a given $p_{T,COR}^{jet}$ bin, $\Delta p_{T,COR}^{jet}$ is the size of the bin, Δy_{CAL}^{jet} denotes the size of the considered region in y_{CAL}^{jet}, and $\mathcal{L}$ is the luminosity. Second, each measurement is corrected for acceptance and smearing effects using a bin-by-bin unfolding procedure, which also accounts for the efficiency of the selection criteria. The unfolding factors, defined as

$$U(p_{T,COR}^{jet}, y_{CAL}^{jet}) = \frac{d^2\sigma/dp_{T,HAD}^{jet} dy_{HAD}^{jet}}{d^2\sigma/dp_{T,COR}^{jet} dy_{CAL}^{jet}}, \tag{4}$$

are extracted from Monte Carlo event samples and applied to the measured $p_{T,COR}^{jet}$ distributions to obtain the final results. The factor $U(p_{T,COR}^{jet}, y_{CAL}^{jet})$ increases with $p_{T,COR}^{jet}$ and shows a moderate y_{CAL}^{jet}-bin dependence. At very low $p_{T,COR}^{jet}$, the unfolding factor varies between 1.02 and 1.06 for different rapidity regions. For jets with $p_{T,COR}^{jet}$ about 300 GeV/c, the factor varies between 1.1 and 1.2, and increases up to 1.3 - 1.4 at very high $p_{T,COR}^{jet}$. In the region $1.1 < |y_{CAL}^{jet}| < 1.6$, the unfolding factor includes an additional correction, $f_U(p_{T,COR}^{jet})$, to account for the fact that the Monte Carlo simulation overestimates the jet momentum resolution in that region (see section VI). The factor $f_U(p_{T,COR}^{jet})$ is computed from Monte Carlo samples as the ratio of the nominal $p_{T,HAD}^{jet}$ distribution smeared using the measured and simulated jet momentum resolution, as determined by the bisector method. The factor $f_U(p_{T,COR}^{jet})$ is about 1.03 and shows no significant $p_{T,COR}^{jet}$ dependence.

IX. SYSTEMATIC UNCERTAINTIES

A detailed study of the systematic uncertainties on the measurements was carried out [36]. Tables III-IV collect the different contributions to the total systematic uncertainty in each p_T^{jet} bin and $|y^{jet}|$ region.

- The measured jet energies were varied by $\pm 2\%$ at low p_T^{jet} to $\pm 3\%$ at high p_T^{jet} to account for the uncertainty on the absolute energy scale in the calorimeter [37]. This introduces an uncertainty on the measured cross sections which varies between $\pm 9\%$ at low p_T^{jet} and $^{+60\%}_{-40\%}$ at high p_T^{jet}.

- Several sources of systematic uncertainty on the ratio β_{DATA}/β_{MC} were considered for the different y^{jet} regions.

  - The uncertainty on the definition of the exclusive dijet sample in data and Monte Carlo events introduces a $\pm 0.5\%$ uncertainty on the absolute energy scale for jets outside the region $0.1 < |y^{jet}| < 0.7$, which translates into an uncertainty on the final results between $\pm 2\%$ at low p_T^{jet} and $\pm 9\%$ at very high p_T^{jet}.

  - The use of different β_{DATA}/β_{MC} parameterizations for jets with $|y^{jet}| > 1.1$ introduces an uncertainty on the final results between $\pm 10\%$ and $\pm 20\%$ at very high p_T^{jet}.

  - In the region $1.1 < |y^{jet}| < 1.6$, an additional -3% uncertainty on the final result, approximately independent of p_T^{jet}, accounts for variations in the β_{DATA}/β_{MC} ratio due to the overestimation of the jet energy resolution in the Monte Carlo samples.

- A $\pm 8\%$ uncertainty on the jet energy resolution introduces an uncertainty on the final results between $\pm 2\%$ at low p_T^{jet} and $\pm 12\%$ at high p_T^{jet}.

- The unfolding procedure was repeated using HERWIG instead of PYTHIA-TUNE A to account for the uncertainty on the modeling of the parton cascades and the jet fragmentation into hadrons. This translates into an uncertainty on the measured cross sections about $\pm 5\%$ at low p_T^{jet}.

- The unfolding procedure was also carried out using unweighted PYTHIA-TUNE A, to estimate the residual dependence on the p_T^{jet} spectra. This introduces an uncertainty of $\pm 4\%$ above 400 GeV/c, which becomes negligible at lower p_T^{jet}.

- The quoted uncertainty on ϵ was taken into account. The effect on the measured cross sections is about $\pm 3\%$ and negligible for jets with p_T^{jet} above 200 GeV/c.

- Other sources of systematic uncertainties related to the selection criteria were found to contribute less than 2% to the total systematic uncertainty.

Positive and negative deviations with respect to the nominal values in each p_T^{jet} bin are added separately in quadrature. Figure 3 shows the total systematic uncertainty on the final results as a function of p_T^{jet} in the different $|y^{jet}|$ regions, where an additional 5.8% uncertainty on the total luminosity is not included.

We plan to produce smooth curves to describe the magnitude of each systematic uncertainty as a function of p_T^{jet} *and avoid statistical fluctuations in the systematics. Therefore quoted numbers at very high* p_T^{jet} *will change slightly.*

X. RESULTS

The measured inclusive jets cross sections, $\frac{d^2\sigma}{dp_T^{jet}dy^{jet}}$, refer to hadron level jets, reconstructed using the k_T algorithm with $D = 0.7$, in the region $p_T^{jet} > 54$ GeV/c and $|y^{jet}| < 2.1$. Figure 4 shows the measured cross sections as a function of p_T^{jet} in five different $|y^{jet}|$ regions compared to NLO pQCD predictions where, for presentation, each measurement has been scaled by a given factor. The data are reported in Tables V-VI. The measured cross sections decrease by more than seven to eight orders of magnitude as p_T^{jet} increases. The NLO pQCD predictions are computed using JETRAD [9] with CTEQ6.1M PDFs [10] and the renormalization and factorization scales (μ_R and μ_F) set to $\mu_0 = \max(p_T^{jet})/2$.

Different sources of uncertainty in the theoretical predictions were considered. The main contribution comes from the uncertainty on the PDFs and was computed using the Hessian method [38]. At low p_T^{jet} the uncertainty is about $\pm 10\%$ and approximately independent of y^{jet}. The uncertainty increases as p_T^{jet} and y^{jet} increase. At very high p_T^{jet}, the uncertainty varies between $^{+60\%}_{-30\%}$ and $^{+140\%}_{-40\%}$ for jets with $|y^{jet}| < 0.1$ and $1.6 < |y^{jet}| < 2.1$, respectively, and is dominated by the limited knowledge of the gluon PDF. An increase of μ_R and μ_F from μ_0 to $2\mu_0$ reduces the theoretical predictions by 2% at low p_T^{jet} and 8% at high p_T^{jet}. Values significantly smaller than μ_0 lead to unstable NLO results and were not considered.

The theoretical predictions include a correction factor, $C_{HAD}(p_T^{jet}, y^{jet})$, that approximately accounts for non-perturbative contributions from the underlying event and fragmentation into hadrons (see Figure 5 and Tables V-VI). In each jet rapidity region, C_{HAD} was estimated, using PYTHIA-TUNE A, as the ratio between the nominal $p_{T,HAD}^{jet}$ distribution and the one obtained by turning off both the interactions between proton and antiproton remnants and the fragmentation in the Monte Carlo samples. The correction decreases as p_T^{jet} increases and shows a moderate y^{jet} dependence. At low p_T^{jet}, C_{HAD} varies between 1.18 and 1.13 as y^{jet} increases, and it becomes of the order of 1.02 at very high p_T^{jet}. The uncertainty on C_{HAD} varies between 12% and 9% at low p_T^{jet} and decreases up to about 1%

at very high p_T^{jet}, as determined from the difference between the parton-to-hadron correction factors obtained using HERWIG instead of PYTHIA-TUNE A.

Figure 6 shows the ratios data/theory as a function of p_T^{jet} in the five different $|y^{jet}|$ regions. Good agreement is observed in the whole range in p_T^{jet} and y^{jet} between the measured cross sections and the theoretical predictions. In particular, no significant deviation from the pQCD prediction is observed for central jets at high p_T^{jet}. In the most forward region, the uncertainty on the theoretical prediction at high p_T^{jet} is larger than that on the measured cross section, which indicates that the data presented in this article will contribute to a better understanding of the gluon PDF. In addition, Figure 6 shows the ratio of pQCD predictions using MRST2004 [11] and CTEQ6.1M PDF sets, well inside the theoretical and experimental uncertainties.

"This section still needs a detailed description of χ^2 tests for data/theory agreement including a long discussion of correlations between systematics in different y^{jet} bins."

For jets in the region $0.1 < |y^{jet}| < 0.7$, the complete analysis is repeated using different values for the D parameter in the k_T algorithm, D = 0.5 and D = 1.0. In both cases, good agreement is observed between the measured cross sections and the NLO pQCD predictions in the whole range in p_T^{jet}. As the D parameter decreases, the measurement becomes less sensitive to the presence and proper modeling of the non-perturbative underlying event contributions. For D = 0.5 (D = 1.0) a parton-to-hadron correction factor $C_{HAD} = 1.1$ ($C_{HAD} = 1.4$) is applied at low p_T^{jet}. This validates the experimental procedure followed to determine the cross section and demonstrates a good control of the parton-to-hadron correction factors applied to the pQCD predictions.

"Here we plan to add the necessary figures and tables for the D=0.5 and D=1.0 measurements"

XI. SUMMARY AND CONCLUSIONS

In summary, we have presented results on inclusive jet production in $p\bar{p}$ collisions at $\sqrt{s} = 1.96$ TeV using the k_T algorithm, for jets with transverse momentum $p_T^{jet} > 54$ GeV/c and rapidity in the region $|y^{jet}| < 2.1$, based on 0.98 fb^{-1} of CDF Run II data. The measured cross sections are in agreement with NLO pQCD predictions after the necessary non-perturbative parton-to-hadron corrections are taken into account. The data presented in this article will contribute to a better understanding of the gluon PDF in the proton.

Acknowledgments

We thank the Fermilab staff and the technical staffs of the participating institutions for their vital contributions. This work was supported by the U.S. Department of Energy and National Science Foundation; the Italian Istituto Nazionale di Fisica Nucleare; the Ministry of Education, Culture, Sports, Science and Technology of Japan; the Natural Sciences and Engineering Research Council of Canada; the National Science Council of the Republic of China; the Swiss National Science Foundation; the A.P. Sloan Foundation; the Bundesministerium fuer Bildung und Forschung, Germany; the Korean Science and Engineering Foundation and the Korean Research Foundation; the Particle Physics and Astronomy Research Council and the Royal Society, UK; the Russian Foundation for Basic Research; the Comision Interministerial de Ciencia y Tecnologia, Spain; in part by the European Community's Human Potential Programme under contract HPRN-CT-2002-00292; and the Academy of Finland.

---

[1] D.J. Gross and F. Wilczek, Phys. Rev. D **8**, 3633 (1973).

H.Fritzsch, M. Gell-Mann and H. Leutwyler, Phys. Lett. **B47**, 365 (1973).

[2] A. Abulencia *et al.* (CDF Collaboration), Phys. Rev. Lett. **96**, 122001 (2006).

[3] A. Abulencia *et al.*, hep-ex/0512020.

[4] T. Affolder *et al.* (CDF Collaboration), Phys. Rev. D **64**, 032001 (2001). [Erratum-ibid. D **65**, 039903 (2002)].

[5] B. Abbott *et al.* (DØ Collaboration), Phys. Rev. Lett. **82**, 2451 (1999).

[6] S. Catani *et al.*, Nucl. Phys. B **406**, 187 (1993).

[7] S.D. Ellis and D.E. Soper, Phys. Rev. D **48**, 3160 (1993).

[8] We use a cylindrical coordinate system about the beam axis in which θ is the polar angle and ϕ is the azimuthal angle. We define $E_T = E\ \sin\theta$, $p_T = p\ \sin\theta$, $\eta = -\ln(\tan(\frac{\theta}{2}))$, and $y = \frac{1}{2}\ln(\frac{\mathrm{E}+\mathrm{p_z}}{\mathrm{E}-\mathrm{p_z}})$.

[9] W.T. Giele, E.W.N. Glover and David A. Kosower, Nucl. Phys. B **403**, 633 (1993).

[10] J. Pumplin *et al.*, JHEP **0207**, 012 (2002).

[11] A. D. Martin *et al.*, Eur. Phys. J. C **23**, 73 (2002).

[12] The hadron level in the Monte Carlo generators is defined using all final-state particles with lifetime above 10^{-11}s.

[13] D. Acosta *et al.* (CDF Collaboration), Phys. Rev. D **71**, 032001 (2005).

[14] A. Sill et al., Nucl. Instrum. Meth. A **447**, 1 (2000).

A. Affolder et al., Nucl. Instrum. Meth. A **453**, 84 (2000).

C.S. Hill, Nucl. Instrum. Meth. A **530**, 1 (2000).

[15] T. Affolder et al., Nucl. Instrum. Meth. A **526**, 249 (2004).

[16] L. Balka *et al.*, Nucl. Instrum. Meth. A **267**, 272 (1988).

[17] S. Bertolucci *et al.*, Nucl. Instrum. Meth. A **267**, 301 (1988).

[18] R. Oishi, Nucl. Instr. Meth. A **453**, 277 (2000).

M. G. Albrow et al., Nucl. Instr. Meth. A **480**, 524 (2002).

[19] D. Acosta *et al.*, Nucl. Instrum. Meth., A **494**, 57 (2002).

[20] B. L. Winer, Int. J. Mod. Phys. A **16S1C**, 1169 (2001).

[21] CDF Collab., F. Abe et al.,Phys. Rev. D **45**, 1448 (1992).

[22] $\not\!\!E_T$ is defined as the norm of $-\sum_i E_T^i \cdot \vec{n}_i$, where $\vec{n}_i$ is the unit vector in the azimuthal plane that points from the beamline to the i-th calorimeter tower.

[23] R. Brun *et al.*, Tech. Rep. CERN-DD/EE/84-1, 1987.

[24] G. Grindhammer, M. Rudowicz and S. Peters, Nucl. Instrum. Meth. A **290**, 469 (1990).

[25] T. Sjöstrand *et al.*, Comp. Phys. Comm. **135**, 238 (2001).

[26] G. Corcella *et al.*, JHEP **0101**, 010 (2001).

[27] H.L. Lai *et al.*, Eur. Phys. J. C **12**, 375 (2000).

[28] PYTHIA-Tune A Monte Carlo samples are generated using the following tuned parameters in PYTHIA: PARP(67) = 4.0, MSTP(82) = 4, PARP(82) = 2.0, PARP(84) = 0.4, PARP(85) = 0.9, PARP(86) = 0.95, PARP(89) = 1800.0, PARP(90) = 0.25.

[29] T. Affolder *et al.* (CDF Collaboration), Phys. Rev. D **65**, 092002 (2002).

[30] D. Acosta *et al.* (CDF Collaboration), Phys. Rev. D **71**, 112002 (2005).

[31] B. Andersson *et al.*, Phys. Rep. **97**, 31 (1983).

[32] T. Sjöstrand, Comp. Phys. Comm. **39**, 347 (1986).

[33] B.R. Webber, Nucl. Phys. B **238**, 492 (1984).

[34] P. Bagnaia *et al.* (UA2 Collaboration), Phys. Lett. B **144**, 283 (1984).

[35] S.R. Hahn *et al.*, Nucl. Instrum. Meth. A **267**, 351 (1988).

[36] Olga Norniella, PhD. Thesis, Universitat Autónoma de Barcelona, in preparation.

[37] A. Bhatti *et al.*, hep-ex/0510047.

[38] J. Pumplin *et al.*, Phys. Rev. D **65**, 014013 (2002).

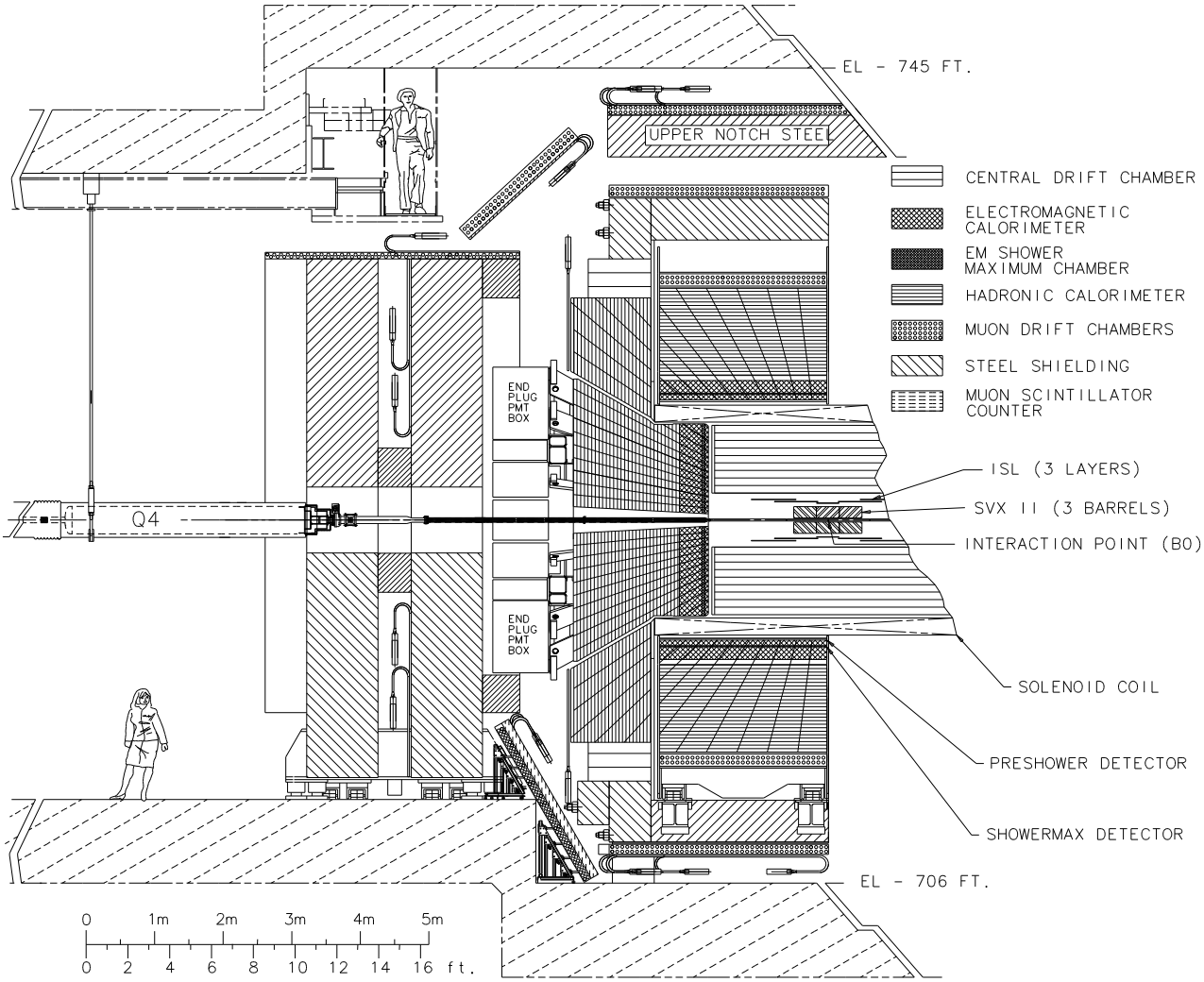

FIG. 1: Longitudinal view of half of the CDF II detector.

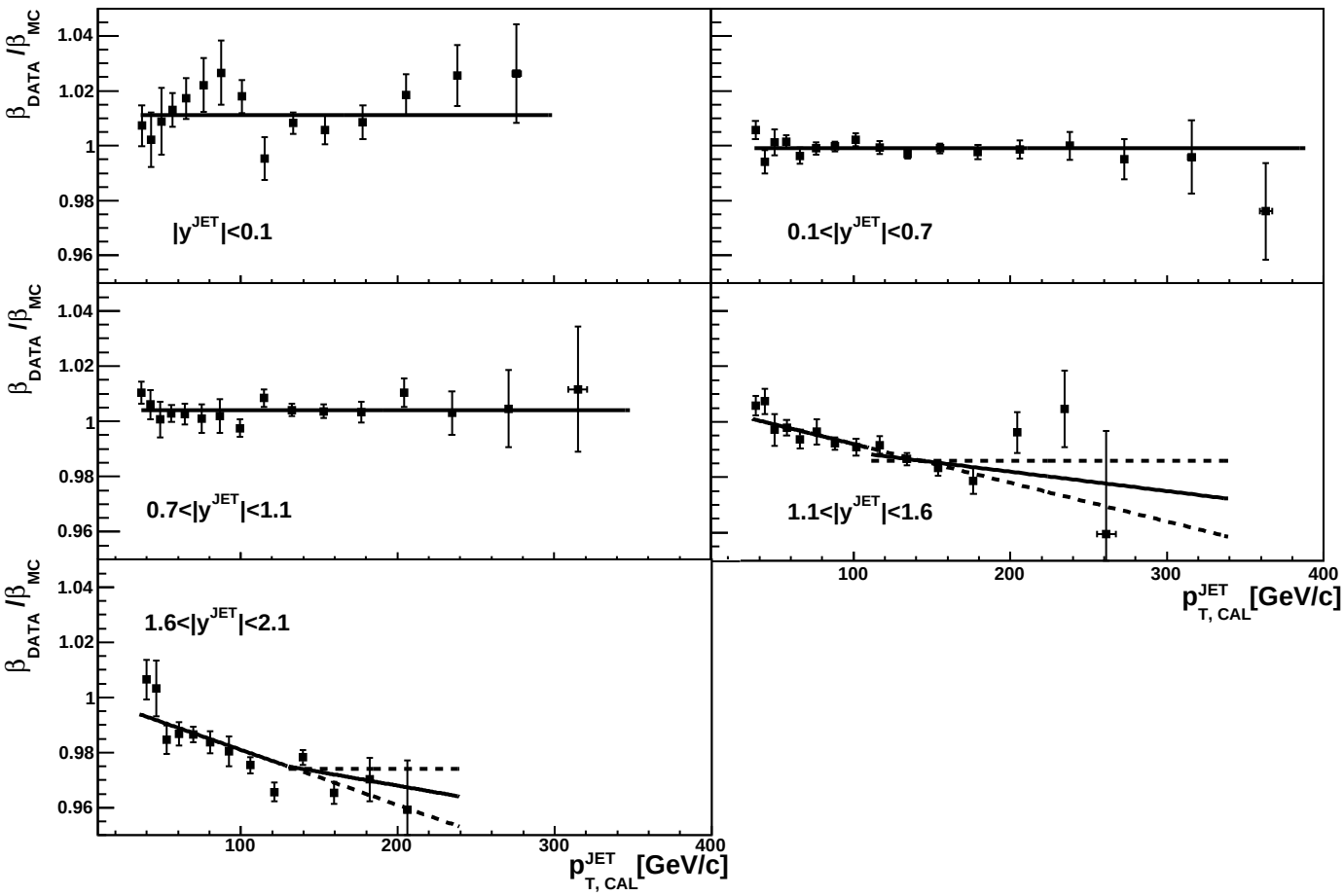

FIG. 2: Ratio $\beta_{\mathrm{DATA}}/\beta_{\mathrm{MC}}$ as a function of $\mathrm{p}^{\mathrm{jet}}_{\mathrm{T,CAL}}$ in different jet rapidity regions. The solid lines are fits to the ratios. In the region $|\mathrm{y}^{\mathrm{jet}}| > 1.1$, the dashed lines indicate different parameterizations used to describe the ratios at high $\mathrm{p}^{\mathrm{jet}}_{\mathrm{T,CAL}}$.

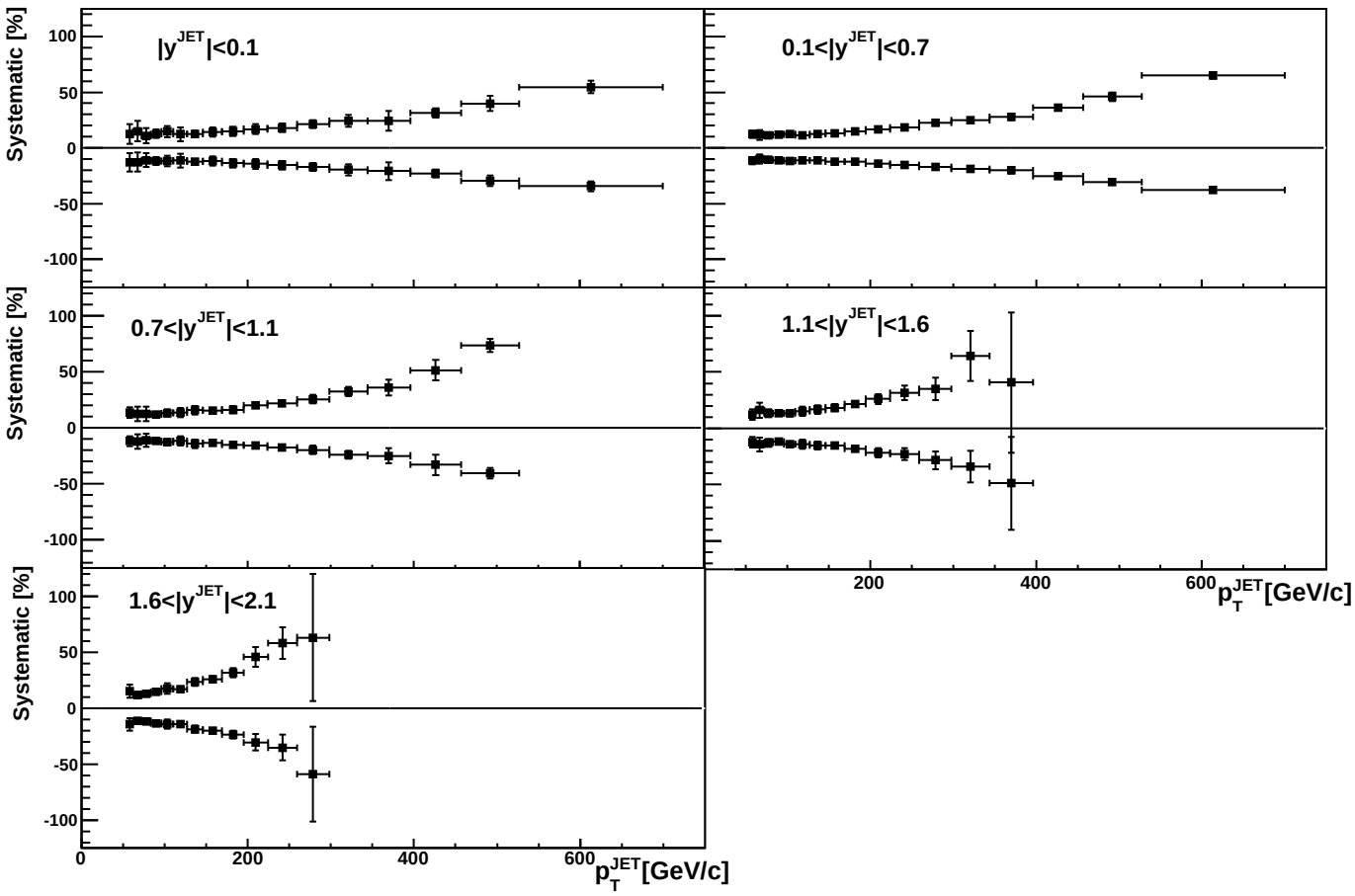

FIG. 3: Total systematic uncertainty (in percentage) on the measured inclusive jet cross sections as a function p_T^{jet} for the different y^{jet} regions.

Syst. Uncertainties ($\lvert y^{jet}\rvert < 0.1$)								
p_T^{jet}	JES	ES(dijet)	p_T^{jet}-balance	resolution	unfolding	pt-spectra	ϵ	selection
54-62	$^{+0.099116}_{-0.09227}$	$^{+0.02843}_{-0.02327}$	-	$^{+0.0422498}_{-0.0527297}$	$^{+0.042959}_{-0.04296}$	$^{+0.0194882}_{-0.01949}$	$^{+0.032749}_{-0.0508}$	$\pm$ 0.02
62-72	$^{+0.10188}_{-0.07137}$	$^{+0.013086}_{-0.01553}$	-	$^{+0.0490551}_{-0.0299562}$	$^{+0.08822}_{-0.08822}$	$^{+0.00870101}_{-0.0087}$	$^{+0.036073}_{-0.04095}$	$\pm$ 0.02
72-83	$^{+0.084514}_{-0.07024}$	$^{+0.021752}_{-0.01576}$	-	$^{+0.0284128}_{-0.0545108}$	$^{+0.045406}_{-0.04541}$	$^{+0.00911716}_{-0.00912}$	$^{+0.030791}_{-0.03688}$	$\pm$ 0.02
83-96	$^{+0.088417}_{-0.07247}$	$^{+0.020932}_{-0.02151}$	-	$^{+0.0352488}_{-0.0277332}$	$^{+0.064634}_{-0.06463}$	$^{+0.0353162}_{-0.03532}$	$^{+0.022716}_{-0.03189}$	$\pm$ 0.02
96-110	$^{+0.121721}_{-0.08536}$	$^{+0.024372}_{-0.01685}$	-	$^{+0.0292584}_{-0.0261106}$	$^{+0.063948}_{-0.06395}$	$^{+0.00940279}_{-0.0094}$	$^{+0.023547}_{-0.03076}$	$\pm$ 0.02
110-127	$^{+0.090212}_{-0.06753}$	$^{+0.019409}_{-0.01907}$	-	$^{+0.0228119}_{-0.0393395}$	$^{+0.072931}_{-0.07293}$	$^{+0.00809653}_{-0.0081}$	$^{+0.01815}_{-0.02566}$	$\pm$ 0.02
127-146	$^{+0.108981}_{-0.10196}$	$^{+0.023002}_{-0.02484}$	-	$^{+0.0194867}_{-0.0224689}$	$^{+0.043029}_{-0.04303}$	$^{+0.0079797}_{-0.00798}$	$^{+0.0187}_{-0.02512}$	$\pm$ 0.02
146-169	$^{+0.131761}_{-0.10585}$	$^{+0.027766}_{-0.02682}$	-	$^{+0.0345299}_{-0.026439}$	$^{+0.017134}_{-0.01713}$	$^{+0.0068154}_{-0.00682}$	$^{+0.014554}_{-0.02255}$	$\pm$ 0.02
169-195	$^{+0.137199}_{-0.11891}$	$^{+0.027486}_{-0.0275}$	-	$^{+0.0256106}_{-0.0402066}$	$^{+0.029624}_{-0.02962}$	$^{+0.0022321}_{-0.00223}$	$^{+0.014139}_{-0.01926}$	$\pm$ 0.02
195-224	$^{+0.152201}_{-0.12612}$	$^{+0.029413}_{-0.02819}$	-	$^{+0.0399064}_{-0.0253346}$	$^{+0.049271}_{-0.04927}$	$^{+0.00859592}_{-0.0086}$	$^{+0.011436}_{-0.01722}$	$\pm$ 0.02
224-259	$^{+0.169088}_{-0.14131}$	$^{+0.031856}_{-0.02916}$	-	$^{+0.0407286}_{-0.0415267}$	$^{+0.025766}_{-0.02577}$	$^{+0.00230163}_{-0.0023}$	$^{+0.013844}_{-0.02001}$	$\pm$ 0.02
259-298	$^{+0.199664}_{-0.15262}$	$^{+0.036444}_{-0.03387}$	-	$^{+0.0436137}_{-0.0439862}$	$^{+0.047826}_{-0.04783}$	$^{+0.000929326}_{-0.00093}$	$^{+0.011505}_{-0.01514}$	$\pm$ 0.02
298-344	$^{+0.232753}_{-0.18352}$	$^{+0.037742}_{-0.03439}$	-	$^{+0.0435852}_{-0.0414134}$	$^{+0.036257}_{-0.03626}$	$^{+0.00160519}_{-0.00161}$	$^{+0.011045}_{-0.01274}$	$\pm$ 0.02
344-396	$^{+0.227553}_{-0.1942}$	$^{+0.037437}_{-0.04407}$	-	$^{+0.0687569}_{-0.0458767}$	$^{+0.021865}_{-0.02186}$	$^{+0.00527694}_{-0.00528}$	$^{+0.005935}_{-0.01187}$	$\pm$ 0.02
396-457	$^{+0.305975}_{-0.21391}$	$^{+0.046868}_{-0.04066}$	-	$^{+0.0453832}_{-0.0510957}$	$^{+0.018303}_{-0.0183}$	$^{+0.0169562}_{-0.01696}$	$^{+0.028037}_{-0.02804}$	$\pm$ 0.02
457-527	$^{+0.384085}_{-0.28087}$	$^{+0.052809}_{-0.06142}$	-	$^{+0.0777365}_{-0.0476934}$	$^{+0.003695}_{-0.0037}$	$^{+0.0449123}_{-0.04491}$	-	$\pm$ 0.02
527-700	$^{+0.530663}_{-0.32223}$	$^{+0.072377}_{-0.067}$	-	$^{+0.0785855}_{-0.0703102}$	$^{+0.003607}_{-0.00361}$	$^{+0.0675625}_{-0.06756}$	-	$\pm$ 0.02

Syst. Uncertainties ($0.1 < \lvert y^{jet}\rvert < 0.7$)								
p_T^{jet}	JES	ES(dijet)	p_T^{jet}-balance	resolution	unfolding	pt-spectra	ϵ	selection
54-62	$^{+0.101711}_{-0.08677}$	—	—	$^{+0.037931}_{-0.03098}$	$^{+0.042667}_{-0.04267}$	$^{+0.007769}_{-0.00777}$	$^{+0.03362}_{-0.04244}$	$\pm$ 0.02
62-72	$^{+0.10375}_{-0.08261}$	—	—	$^{+0.037146}_{-0.03532}$	$^{+0.016035}_{-0.01604}$	$^{+0.006372}_{-0.00637}$	$^{+0.030356}_{-0.03903}$	$\pm$ 0.02
72-83	$^{+0.098657}_{-0.08459}$	—	—	$^{+0.030102}_{-0.02928}$	$^{+0.040244}_{-0.04024}$	$^{+0.005073}_{-0.00507}$	$^{+0.027963}_{-0.03757}$	$\pm$ 0.02
83-96	$^{+0.102166}_{-0.09073}$	—	—	$^{+0.029476}_{-0.02518}$	$^{+0.039526}_{-0.03953}$	$^{+0.00508}_{-0.00508}$	$^{+0.022877}_{-0.03188}$	$\pm$ 0.02
96-110	$^{+0.108636}_{-0.09503}$	—	—	$^{+0.020562}_{-0.02062}$	$^{+0.050665}_{-0.05066}$	$^{+0.005379}_{-0.00538}$	$^{+0.021745}_{-0.03019}$	$\pm$ 0.02
110-127	$^{+0.10157}_{-0.09706}$	—	—	$^{+0.025326}_{-0.02177}$	$^{+0.029413}_{-0.02941}$	$^{+0.00462}_{-0.00462}$	$^{+0.019006}_{-0.02647}$	$\pm$ 0.02
127-146	$^{+0.116123}_{-0.10107}$	—	—	$^{+0.017551}_{-0.01593}$	$^{+0.025511}_{-0.02551}$	$^{+0.004668}_{-0.00467}$	$^{+0.016763}_{-0.02412}$	$\pm$ 0.02
146-169	$^{+0.126603}_{-0.113}$	—	—	$^{+0.024647}_{-0.0209}$	$^{+0.024915}_{-0.02491}$	$^{+0.004913}_{-0.00491}$	$^{+0.015983}_{-0.02213}$	$\pm$ 0.02
169-195	$^{+0.144268}_{-0.11782}$	—	—	$^{+0.021155}_{-0.02002}$	$^{+0.020206}_{-0.02021}$	$^{+0.004367}_{-0.00437}$	$^{+0.014145}_{-0.02071}$	$\pm$ 0.02
195-224	$^{+0.161181}_{-0.13445}$	—	—	$^{+0.026257}_{-0.02625}$	$^{+0.025843}_{-0.02584}$	$^{+0.003744}_{-0.00374}$	$^{+0.012745}_{-0.01772}$	$\pm$ 0.02
224-259	$^{+0.177476}_{-0.1468}$	—	—	$^{+0.029338}_{-0.02656}$	$^{+0.032603}_{-0.0326}$	$^{+0.003138}_{-0.00314}$	$^{+0.012262}_{-0.01878}$	$\pm$ 0.02
259-298	$^{+0.221563}_{-0.1666}$	—	—	$^{+0.031125}_{-0.03103}$	$^{+0.007626}_{-0.00763}$	$^{+0.002612}_{-0.00261}$	$^{+0.011737}_{-0.01596}$	$\pm$ 0.02
298-344	$^{+0.243694}_{-0.18341}$	—	—	$^{+0.038115}_{-0.0334}$	$^{+0.02004}_{-0.02004}$	$^{+0.002492}_{-0.00249}$	$^{+0.013379}_{-0.01729}$	$\pm$ 0.02
344-396	$^{+0.27388}_{-0.1922}$	—	—	$^{+0.042404}_{-0.03743}$	$^{+0.025039}_{-0.02504}$	$^{+0.003158}_{-0.00316}$	$^{+0.011682}_{-0.01285}$	$\pm$ 0.02
396-457	$^{+0.359754}_{-0.24884}$	—	—	$^{+0.04796}_{-0.04348}$	$^{+0.007703}_{-0.0077}$	$^{+0.007651}_{-0.00765}$	$^{+0.007712}_{-0.02314}$	$\pm$ 0.02
457-527	$^{+0.454697}_{-0.29681}$	—	—	$^{+0.063566}_{-0.06206}$	$^{+0.035493}_{-0.03549}$	$^{+0.016904}_{-0.0169}$	—	$\pm$ 0.02
527-700	$^{+0.643912}_{-0.36897}$	—	—	$^{+0.084383}_{-0.07394}$	$^{+0.008521}_{-0.00852}$	$^{+0.035742}_{-0.03574}$	—	$\pm$ 0.02

TABLE III: Fractional contributions to the total systematic uncertainty on the measured inclusive jet differential cross section as a function of p_T^{jet} for jets in the regions $|y^{jet}| < 0.1$ and $0.1 < |y^{jet}| < 0.7$.

Syst. Uncertainties ($0.7 < \lvert y^{jet} \rvert < 1.1$)								
p_T^{jet}	JES	ES(dijet)	p_T^{jet}-balance	resolution	unfolding	pt-spectra	ϵ	selection
54-62	$^{+0.106696}_{-0.08342}$	$^{+0.023687}_{-0.02202}$	–	$^{+0.046162}_{-0.03946}$	$^{+0.054062}_{-0.05406}$	$^{+0.008986}_{-0.00899}$	$^{+0.032817}_{-0.04328}$	± 0.02
62-72	$^{+0.090257}_{-0.08593}$	$^{+0.021158}_{-0.02458}$	–	$^{+0.045645}_{-0.04396}$	$^{+0.051801}_{-0.0518}$	$^{+0.01509}_{-0.01509}$	$^{+0.033017}_{-0.04143}$	± 0.02
72-83	$^{+0.103142}_{-0.08332}$	$^{+0.024289}_{-0.02087}$	–	$^{+0.04153}_{-0.03949}$	$^{+0.022927}_{-0.02293}$	$^{+0.028848}_{-0.02885}$	$^{+0.025721}_{-0.03795}$	± 0.02
83-96	$^{+0.096246}_{-0.09007}$	$^{+0.022514}_{-0.0258}$	–	$^{+0.031566}_{-0.03296}$	$^{+0.049986}_{-0.04999}$	$^{+0.006606}_{-0.00661}$	$^{+0.023828}_{-0.03562}$	± 0.02
96-110	$^{+0.110682}_{-0.1062}$	$^{+0.025523}_{-0.0264}$	–	$^{+0.035881}_{-0.03364}$	$^{+0.035699}_{-0.0357}$	$^{+0.025515}_{-0.02551}$	$^{+0.024891}_{-0.02971}$	± 0.02
110-127	$^{+0.119743}_{-0.0953}$	$^{+0.026048}_{-0.02634}$	–	$^{+0.028639}_{-0.02669}$	$^{+0.028646}_{-0.02865}$	$^{+0.03226}_{-0.03226}$	$^{+0.01715}_{-0.02734}$	± 0.02
127-146	$^{+0.121427}_{-0.10213}$	$^{+0.026693}_{-0.02339}$	–	$^{+0.042279}_{-0.03657}$	$^{+0.063745}_{-0.06375}$	$^{+0.054563}_{-0.05456}$	$^{+0.018398}_{-0.02516}$	± 0.02
146-169	$^{+0.142164}_{-0.12193}$	$^{+0.025341}_{-0.0289}$	–	$^{+0.029226}_{-0.03044}$	$^{+0.021826}_{-0.02183}$	$^{+0.012866}_{-0.01287}$	$^{+0.016547}_{-0.02403}$	± 0.02
169-195	$^{+0.148021}_{-0.13781}$	$^{+0.02806}_{-0.02873}$	–	$^{+0.025487}_{-0.02732}$	$^{+0.04008}_{-0.04008}$	$^{+0.023966}_{-0.02397}$	$^{+0.015614}_{-0.0228}$	± 0.02
195-224	$^{+0.186474}_{-0.14493}$	$^{+0.034746}_{-0.03316}$	–	$^{+0.039932}_{-0.03611}$	$^{+0.022275}_{-0.02227}$	$^{+0.02766}_{-0.02766}$	$^{+0.014748}_{-0.01829}$	± 0.02
224-259	$^{+0.210582}_{-0.1626}$	$^{+0.034196}_{-0.0342}$	–	$^{+0.038651}_{-0.0402}$	$^{+0.015059}_{-0.01506}$	$^{+0.003357}_{-0.00336}$	$^{+0.013668}_{-0.02082}$	± 0.02
259-298	$^{+0.244812}_{-0.18526}$	$^{+0.039484}_{-0.03987}$	–	$^{+0.055706}_{-0.04244}$	$^{+0.010254}_{-0.01025}$	$^{+0.001127}_{-0.00113}$	$^{+0.012378}_{-0.01749}$	± 0.02
298-344	$^{+0.314049}_{-0.22338}$	$^{+0.052665}_{-0.04632}$	–	$^{+0.054099}_{-0.05132}$	$^{+0.028379}_{-0.02838}$	$^{+0.018298}_{-0.0183}$	$^{+0.007076}_{-0.02241}$	± 0.02
344-396	$^{+0.344149}_{-0.23131}$	$^{+0.053233}_{-0.04751}$	–	$^{+0.075507}_{-0.0674}$	$^{+0.026362}_{-0.02636}$	$^{+0.000138}_{-0.00014}$	$^{+0.017964}_{-0.01497}$	± 0.02
396-457	$^{+0.500999}_{-0.30885}$	$^{+0.067951}_{-0.06725}$	–	$^{+0.077586}_{-0.07573}$	$^{+0.01249}_{-0.01249}$	$^{+0.033921}_{-0.03392}$	–	± 0.02
457-527	$^{+0.715452}_{-0.38005}$	$^{+0.091315}_{-0.08416}$	–	$^{+0.121313}_{-0.09427}$	$^{+0.001828}_{-0.00183}$	$^{+0.059751}_{-0.05975}$	–	± 0.02

Syst. Uncertainties ($1.1 < \lvert y^{jet} \rvert < 1.6$)								
p_T^{jet}	JES	ES(dijet)	p_T^{jet}-balance	resolution	unfolding	pt-spectra	ϵ	selection
54-62	$^{+0.085893}_{-0.08066}$	$^{+0.023527}_{-0.0255516}$	x	$^{+0.039218}_{-0.03269}$	$^{+0.057239}_{-0.05724}$	$^{+0.015593}_{-0.01559}$	$^{+0.037516}_{-0.04868}$	± 0.02
62-72	$^{+0.12831}_{-0.0951}$	$^{+0.027942}_{-0.024855}$	x	$^{+0.034607}_{-0.04111}$	$^{+0.077137}_{-0.07714}$	$^{+0.012487}_{-0.01249}$	$^{+0.033616}_{-0.04277}$	± 0.02
72-83	$^{+0.102713}_{-0.0896}$	$^{+0.025302}_{-0.0243952}$	x	$^{+0.027355}_{-0.02485}$	$^{+0.065687}_{-0.06569}$	$^{+0.010476}_{-0.01048}$	$^{+0.031588}_{-0.04134}$	± 0.02
83-96	$^{+0.106742}_{-0.07956}$	$^{+0.024324}_{-0.0177289}$	x	$^{+0.031031}_{-0.03126}$	$^{+0.061985}_{-0.06198}$	$^{+0.001392}_{-0.00139}$	$^{+0.026435}_{-0.02602}$	± 0.02
96-110	$^{+0.114864}_{-0.11238}$	$^{+0.024533}_{-0.0305982}$	x	$^{+0.027738}_{-0.02819}$	$^{+0.051429}_{-0.05143}$	$^{+0.008977}_{-0.00898}$	$^{+0.025538}_{-0.03251}$	± 0.02
110-127	$^{+0.127172}_{-0.10606}$	$^{+0.025477}_{-0.0263097}$	x	$^{+0.029929}_{-0.04266}$	$^{+0.063391}_{-0.06339}$	$^{+0.007678}_{-0.00768}$	$^{+0.021798}_{-0.03095}$	± 0.02
127-146	$^{+0.147559}_{-0.1266}$	$^{+0.030326}_{-0.0281929}$	x	$^{+0.033492}_{-0.02612}$	$^{+0.055058}_{-0.05506}$	$^{+0.006271}_{-0.00627}$	$^{+0.020791}_{-0.02869}$	± 0.02
146-169	$^{+0.170083}_{-0.13475}$	$^{+0.035661}_{-0.0319929}$	x	$^{+0.04119}_{-0.03224}$	$^{+0.031275}_{-0.03128}$	$^{+0.003995}_{-0.004}$	$^{+0.01982}_{-0.02605}$	± 0.02
169-195	$^{+0.195442}_{-0.15413}$	$^{+0.037444}_{-0.0355699}$	x	$^{+0.0435}_{-0.05164}$	$^{+0.05929}_{-0.05929}$	$^{+0.001499}_{-0.0015}$	$^{+0.017965}_{-0.02517}$	± 0.02
195-224	$^{+0.234984}_{-0.18451}$	$^{+0.045742}_{-0.0423148}$	x	$^{+0.056036}_{-0.04683}$	$^{+0.083102}_{-0.0831}$	$^{+0.002662}_{-0.00266}$	$^{+0.018388}_{-0.02733}$	± 0.02
224-259	$^{+0.303443}_{-0.20955}$	$^{+0.044662}_{-0.0470138}$	x	$^{+0.059553}_{-0.06043}$	$^{+0.020641}_{-0.02064}$	$^{+0.016502}_{-0.0165}$	$^{+0.01848}_{-0.0239}$	± 0.02
259-298	$^{+0.330725}_{-0.2561}$	$^{+0.052204}_{-0.0496697}$	x	$^{+0.062429}_{-0.05658}$	$^{+0.062103}_{-0.0621}$	$^{+0.016601}_{-0.0166}$	$^{+0.017784}_{-0.02941}$	± 0.02
298-344	$^{+0.583972}_{-0.28365}$	$^{+0.133409}_{-0.0744141}$	x	$^{+0.103189}_{-0.09403}$	$^{+0.071251}_{-0.07125}$	$^{+0.0308}_{-0.0308}$	$^{+0.03125}_{-0.02734}$	± 0.02
344-396	$^{+0.38352}_{-0.40192}$	$^{+0}_{-0.129358}$	x	$^{+0.091363}_{-0.10474}$	$^{+0.040007}_{-0.04001}$	$^{+0.056124}_{-0.05612}$	–	± 0.02

Syst. Uncertainties ($1.6 < \lvert y^{jet} \rvert < 2.1$)								
p_T^{jet}	JES	ES(dijet)	p_T^{jet}-balance	resolution	unfolding	pt-spectra	ϵ	selection
54-62	$^{+0.124809}_{-0.10845}$	$^{+0.025559}_{-0.02778}$	–	$^{+0.019417}_{-0.02122}$	$^{+0.067723}_{-0.06772}$	$^{+0.013274}_{-0.01327}$	$^{+0.039299}_{-0.04834}$	± 0.02
62-72	$^{+0.10224}_{-0.09156}$	$^{+0.023586}_{-0.02266}$	–	$^{+0.016903}_{-0.01509}$	$^{+0.025756}_{-0.02576}$	$^{+0.00861}_{-0.00861}$	$^{+0.032072}_{-0.04726}$	± 0.02
72-83	$^{+0.119068}_{-0.09846}$	$^{+0.028795}_{-0.02544}$	–	$^{+0.017156}_{-0.01728}$	$^{+0.022573}_{-0.02257}$	$^{+0.007727}_{-0.00773}$	$^{+0.030187}_{-0.04121}$	± 0.02
83-96	$^{+0.12762}_{-0.1114}$	$^{+0.027232}_{-0.02725}$	–	$^{+0.01226}_{-0.01467}$	$^{+0.049963}_{-0.04996}$	$^{+0.004896}_{-0.0049}$	$^{+0.028716}_{-0.03714}$	± 0.02
96-110	$^{+0.165592}_{-0.12783}$	$^{+0.034049}_{-0.03093}$	–	$^{+0.01802}_{-0.01418}$	$^{+0.030497}_{-0.0305}$	$^{+0.003444}_{-0.00344}$	$^{+0.02454}_{-0.0383}$	± 0.02
110-127	$^{+0.15956}_{-0.13217}$	$^{+0.032854}_{-0.03072}$	–	$^{+0.010174}_{-0.0146}$	$^{+0.020221}_{-0.02022}$	$^{+0.003872}_{-0.00387}$	$^{+0.02679}_{-0.0356}$	± 0.02
127-146	$^{+0.225331}_{-0.17243}$	$^{+0.044099}_{-0.0438}$	–	$^{+0.018944}_{-0.02012}$	$^{+0.035764}_{-0.03576}$	$^{+0.003563}_{-0.00356}$	$^{+0.024612}_{-0.03282}$	± 0.02
146-169	$^{+0.247366}_{-0.18799}$	$^{+0.046112}_{-0.04448}$	–	$^{+0.021542}_{-0.01862}$	$^{+0.042828}_{-0.04283}$	$^{+0.005737}_{-0.00574}$	$^{+0.024809}_{-0.03376}$	± 0.02
169-195	$^{+0.305518}_{-0.21901}$	$^{+0.048681}_{-0.05128}$	$^{+0.008765}_{-0.01325}$	$^{+0.025774}_{-0.03013}$	$^{+0.051599}_{-0.0516}$	$^{+0.012614}_{-0.01261}$	$^{+0.025926}_{-0.03258}$	± 0.02
195-224	$^{+0.443437}_{-0.28647}$	$^{+0.077106}_{-0.06481}$	$^{+0.060031}_{-0.05201}$	$^{+0.030115}_{-0.02949}$	$^{+0.029961}_{-0.02996}$	$^{+0.006109}_{-0.00611}$	$^{+0.027641}_{-0.0385}$	± 0.02
224-259	$^{+0.560925}_{-0.3259}$	$^{+0.076733}_{-0.078}$	$^{+0.123737}_{-0.09404}$	$^{+0.034804}_{-0.03437}$	$^{+0.034881}_{-0.03488}$	$^{+0.007328}_{-0.00733}$	$^{+0.038793}_{-0.03017}$	± 0.02
259-298	$^{+0.559045}_{-0.47689}$	$^{+0.084139}_{-0.15693}$	$^{+0.230133}_{-0.25417}$	$^{+0.054791}_{-0.04458}$	$^{+0.109084}_{-0.10908}$	$^{+0.104713}_{-0.10471}$	–	± 0.02

TABLE IV: Fractional contributions to the total systematic uncertainty on the measured inclusive jet differential cross section as a function of p_T^{jet} for jets in the regions $0.7 < |y^{jet}| < 1.1$, $1.1 < |y^{jet}| < 1.6$, and $1.6 < |y^{jet}| < 2.1$.

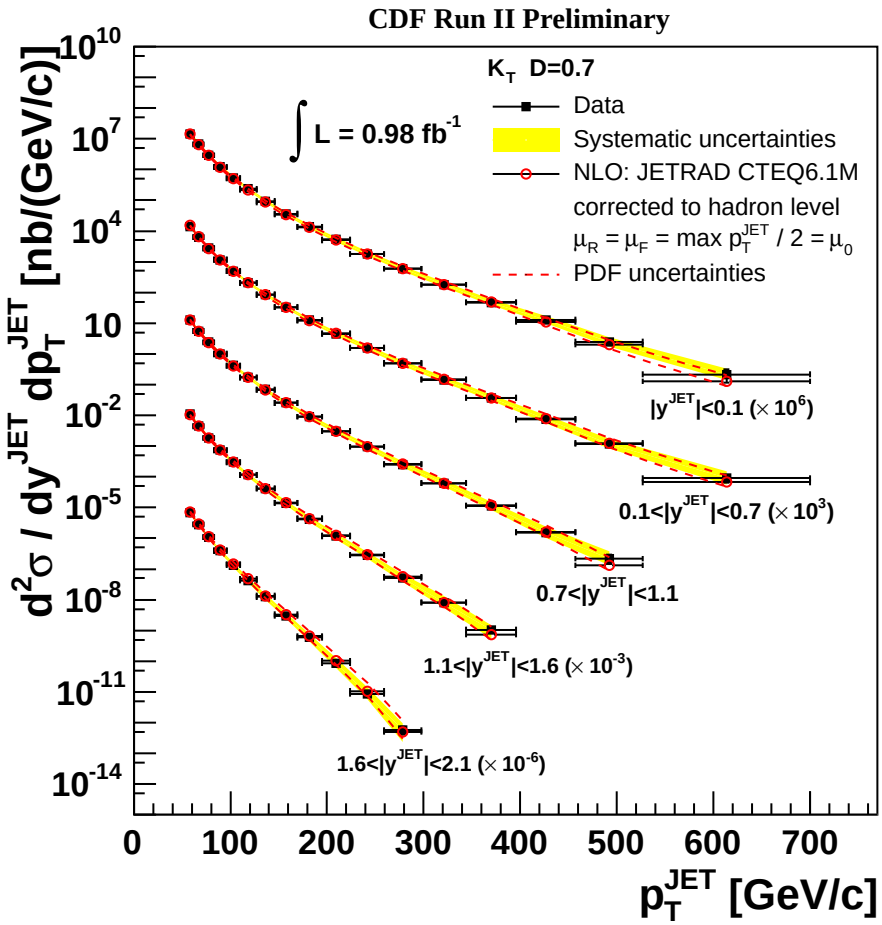

FIG. 4: Measured inclusive jet cross sections (black dots) as a function of p_T^{jet} for jets with $p_T^{jet} > 54$ GeV/c in different y^{jet} regions compared to NLO pQCD predictions (open circles). The shaded band shows the total systematic uncertainty on the measurement. A 5.8% uncertainty on the luminosity is not included. The dashed lines indicate the PDF uncertainty on the theoretical predictions. For presentation, each measurement is scaled by a given factor.

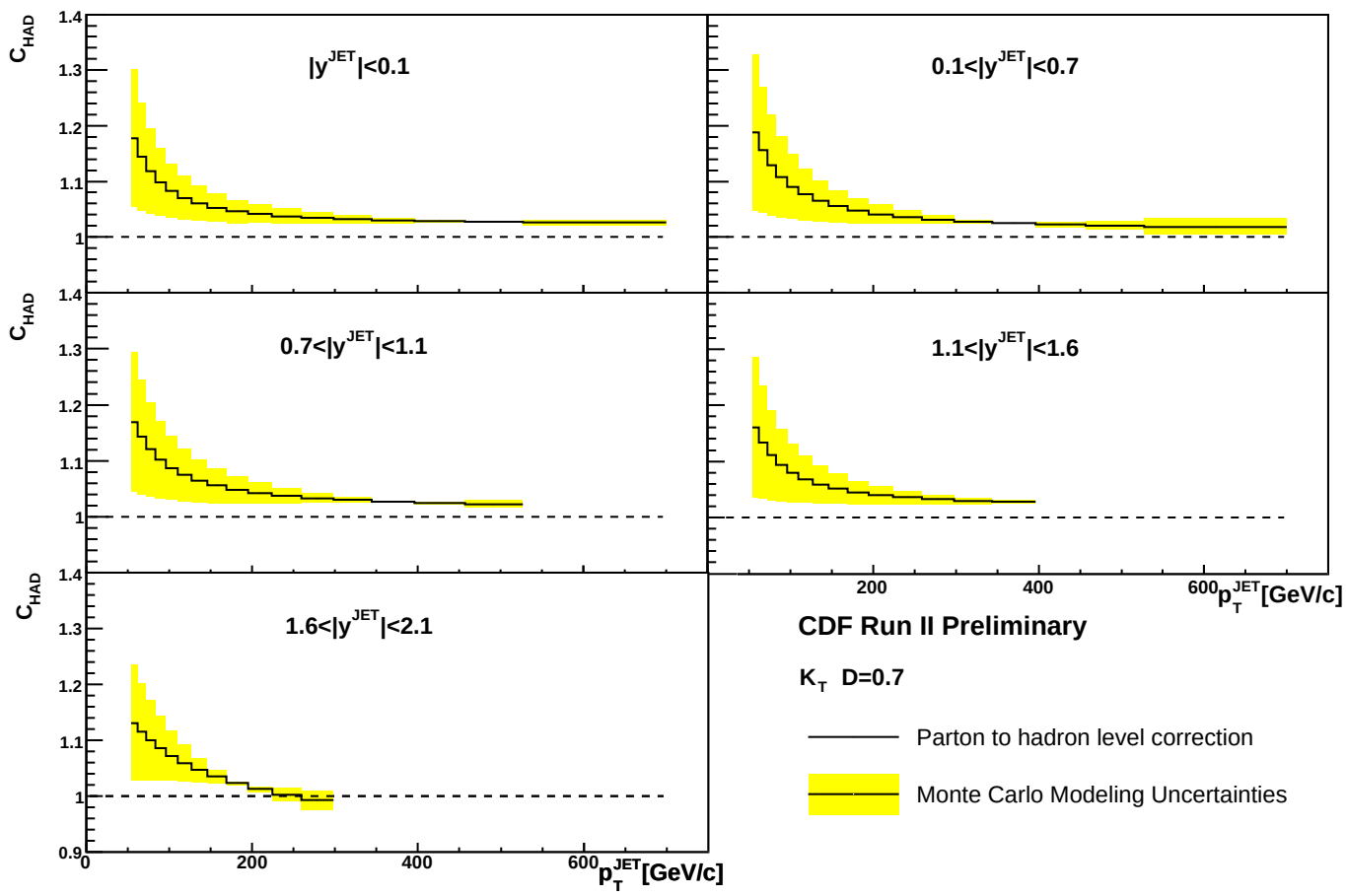

FIG. 5: Magnitude of the parton-to-hadron correction, $C_{\mathrm{HAD}}(\mathrm{p_T^{jet}}, \mathrm{y^{jet}})$, used to correct the NLO pQCD predictions. The shaded band indicates the quoted Monte Carlo modeling uncertainty.

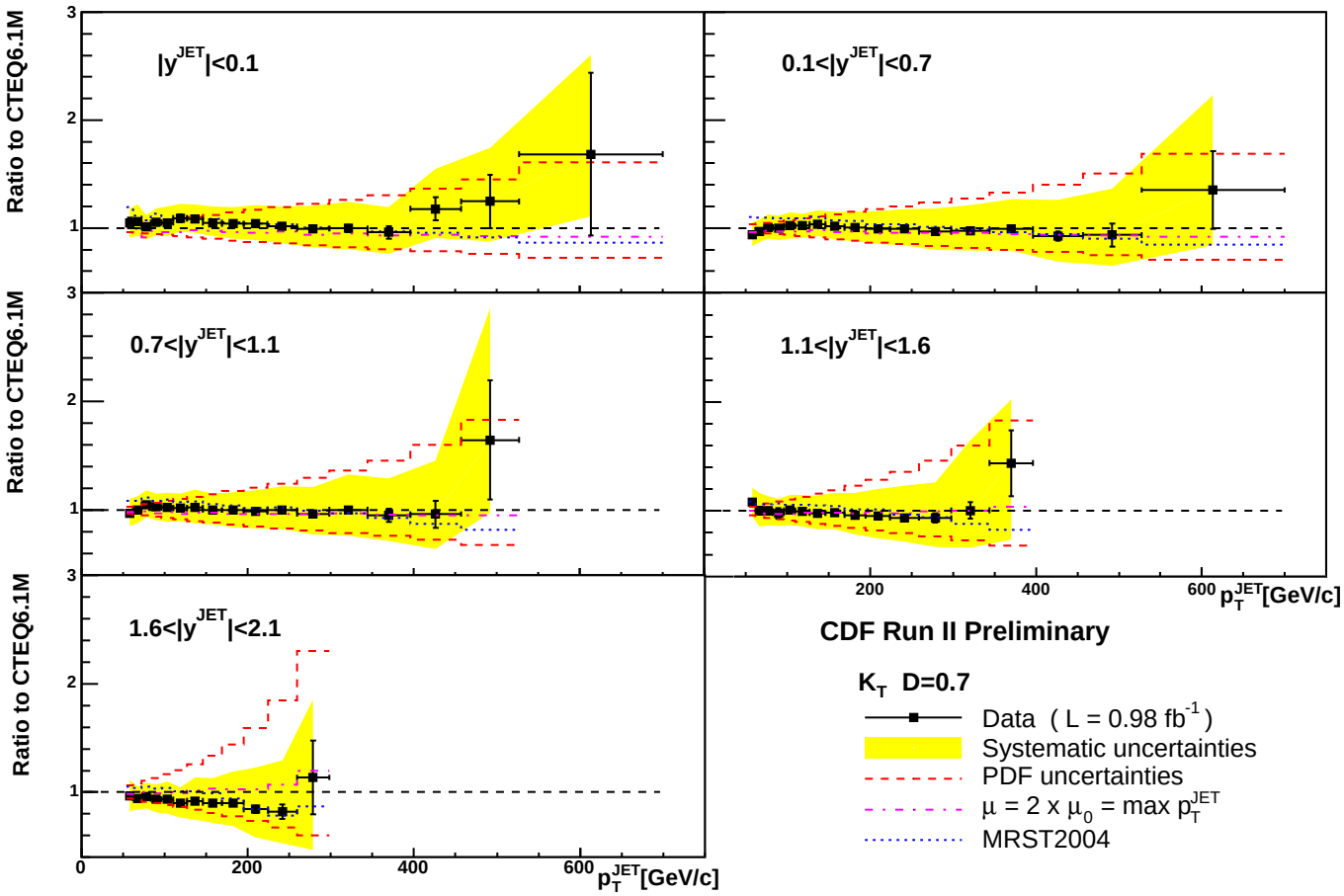

FIG. 6: Ratio Data/Theory as a function of p_T^{jet} in different y^{jet} regions. The error bars (shaded band) show the total statistical (systematic) uncertainty on the data. A 5.8% uncertainty on the luminosity is not included. The dashed lines indicate the PDF uncertainty on the theoretical prediction. The dotted line presents the ratio of MRST2004 and CTEQ6.1M predictions. The dotted-dashed line shows the ratio of predictions with $2\mu_0$ and μ_0.

$\frac{d^2\sigma}{dp_T^{jet}dy^{jet}}$ $(\lvert y^{jet}\rvert < 0.1)$		
p_T^{jet} [GeV/c]	$\sigma \pm$ (stat.) $\pm$ (sys.) [nb/(GeV/c)]	C_{HAD} parton $\rightarrow$ hadron
54 - 62	$(14.7 \pm 0.5^{+1.9}_{-1.9}) \times 10^{0}$	1.177 ± 0.124
62 - 72	$(6.77 \pm 0.08^{+1.02}_{-0.86}) \times 10^{0}$	1.144 ± 0.097
72 - 83	$(2.91 \pm 0.05^{+0.32}_{-0.32}) \times 10^{0}$	1.118 ± 0.077
83 - 96	$(1.25 \pm 0.02^{+0.16}_{-0.14}) \times 10^{0}$	1.098 ± 0.061
96 - 110	$(5.37 \pm 0.11^{+0.78}_{-0.63}) \times 10^{-1}$	1.083 ± 0.049
110 - 127	$(2.35 \pm 0.06^{+0.29}_{-0.27}) \times 10^{-1}$	1.070 ± 0.039
127 - 146	$(9.43 \pm 0.12^{+1.17}_{-1.13}) \times 10^{-2}$	1.060 ± 0.031
146 - 169	$(3.65 \pm 0.06^{+0.52}_{-0.43}) \times 10^{-2}$	1.052 ± 0.025
169 - 195	$(1.39 \pm 0.01^{+0.20}_{-0.19}) \times 10^{-2}$	1.046 ± 0.020
195 - 224	$(5.24 \pm 0.06^{+0.89}_{-0.75}) \times 10^{-3}$	1.041 ± 0.017
224 - 259	$(1.80 \pm 0.03^{+0.33}_{-0.28}) \times 10^{-3}$	1.037 ± 0.013
259 - 298	$(5.93 \pm 0.11^{+1.27}_{-1.00}) \times 10^{-4}$	1.034 ± 0.010
298 - 344	$(1.79 \pm 0.06^{+0.44}_{-0.35}) \times 10^{-4}$	1.032 ± 0.007
344 - 396	$(4.69 \pm 0.28^{+1.14}_{-0.97}) \times 10^{-5}$	1.030 ± 0.005
396 - 457	$(1.30 \pm 0.12^{+0.41}_{-0.30}) \times 10^{-5}$	1.028 ± 0.002
457 - 527	$(2.47 \pm 0.50^{+0.98}_{-0.73}) \times 10^{-6}$	1.027 ± 0.001
527 - 700	$(2.14 \pm 0.96^{+1.17}_{-0.74}) \times 10^{-7}$	1.026 ± 0.005

$\frac{d^2\sigma}{dp_T^{jet}dy^{jet}}$ $(0.1 < \lvert y^{jet}\rvert < 0.7)$		
p_T^{jet} [GeV/c]	$\sigma \pm$ (stat.) $\pm$ (sys.) [nb/(GeV/c)]	C_{HAD} parton $\rightarrow$ hadron
54 - 62	$(14.2 \pm 0.2^{+1.7}_{-1.6}) \times 10^{0}$	1.188 ± 0.140
62 - 72	$(6.23 \pm 0.12^{+0.73}_{-0.63}) \times 10^{0}$	1.155 ± 0.113
72 - 83	$(2.73 \pm 0.02^{+0.32}_{-0.29}) \times 10^{0}$	1.129 ± 0.091
83 - 96	$(1.15 \pm 0.01^{+0.13}_{-0.12}) \times 10^{0}$	1.108 ± 0.073
96 - 110	$(4.96 \pm 0.04^{+0.62}_{-0.57}) \times 10^{-1}$	1.090 ± 0.059
110 - 127	$(2.09 \pm 0.02^{+0.23}_{-0.23}) \times 10^{-1}$	1.076 ± 0.047
127 - 146	$(8.58 \pm 0.04^{+1.06}_{-0.95}) \times 10^{-2}$	1.065 ± 0.037
146 - 169	$(3.35 \pm 0.02^{+0.45}_{-0.41}) \times 10^{-2}$	1.055 ± 0.029
169 - 195	$(1.24 \pm 0.01^{+0.18}_{-0.15}) \times 10^{-2}$	1.047 ± 0.022
195 - 224	$(4.56 \pm 0.02^{+0.76}_{-0.65}) \times 10^{-3}$	1.041 ± 0.017
224 - 259	$(1.58 \pm 0.01^{+0.29}_{-0.24}) \times 10^{-3}$	1.036 ± 0.012
259 - 298	$(4.89 \pm 0.06^{+1.10}_{-0.84}) \times 10^{-4}$	1.031 ± 0.007
298 - 344	$(1.43 \pm 0.02^{+0.36}_{-0.27}) \times 10^{-4}$	1.028 ± 0.003
344 - 396	$(3.71 \pm 0.01^{+1.04}_{-0.74}) \times 10^{-5}$	1.025 ± 0.001
396 - 457	$(7.27 \pm 0.34^{+2.65}_{-1.90}) \times 10^{-6}$	1.023 ± 0.004
457 - 527	$(1.17 \pm 0.13^{+0.54}_{-0.36}) \times 10^{-6}$	1.021 ± 0.008
527 - 700	$(9.01 \pm 2.41^{+5.86}_{-3.40}) \times 10^{-8}$	1.018 ± 0.014

TABLE V: Measured inclusive jet differential cross section as a function of p_T^{jet} for jets in the regions $|y^{jet}| < 0.1$ and $0.1 < |y^{jet}| < 0.7$. An additional 5.8% uncertainty on the luminosity is not included. The parton-to-hadron correction factors, $C_{HAD}(p_T^{jet})$, are applied to the pQCD predictions.

$\frac{d^2\sigma}{dp_T^{jet}dy^{jet}}$ $(0.7 < \lvert y^{jet}\rvert < 1.1)$		
p_T^{jet} [GeV/c]	$\sigma \pm$ (stat.) $\pm$ (sys.) [nb/(GeV/c)]	C_{HAD} parton $\rightarrow$ hadron
54 - 62	$(12.4 \pm 0.2^{+1.7}_{-1.5}) \times 10^{0}$	1.169 ± 0.125
62 - 72	$(5.54 \pm 0.14^{+0.68}_{-0.68}) \times 10^{0}$	1.143 ± 0.103
72 - 83	$(2.42 \pm 0.02^{+0.30}_{-0.27}) \times 10^{0}$	1.120 ± 0.084
83 - 96	$(1.01 \pm 0.01^{+0.12}_{-0.12}) \times 10^{0}$	1.102 ± 0.070
96 - 110	$(4.18 \pm 0.05^{+0.55}_{-0.53}) \times 10^{-1}$	1.087 ± 0.057
110 - 127	$(1.74 \pm 0.03^{+0.24}_{-0.20}) \times 10^{-1}$	1.075 ± 0.047
127 - 146	$(6.87 \pm 0.05^{+1.09}_{-0.98}) \times 10^{-2}$	1.064 ± 0.038
146 - 169	$(2.53 \pm 0.03^{+0.38}_{-0.34}) \times 10^{-2}$	1.056 ± 0.031
169 - 195	$(9.00 \pm 0.06^{+1.45}_{-1.38}) \times 10^{-3}$	1.048 ± 0.024
195 - 224	$(3.05 \pm 0.02^{+0.61}_{-0.48}) \times 10^{-3}$	1.042 ± 0.019
224 - 259	$(9.56 \pm 0.01^{+2.09}_{-1.66}) \times 10^{-4}$	1.037 ± 0.014
259 - 298	$(2.54 \pm 0.05^{+0.65}_{-0.50}) \times 10^{-4}$	1.033 ± 0.009
298 - 344	$(6.23 \pm 0.17^{+0.20}_{-1.48}) \times 10^{-5}$	1.030 ± 0.005
344 - 396	$(1.12 \pm 0.07^{+0.40}_{-0.28}) \times 10^{-5}$	1.027 ± 0.001
396 - 457	$(1.56 \pm 0.20^{+0.80}_{-0.51}) \times 10^{-6}$	1.025 ± 0.003
457 - 527	$(2.18 \pm 0.73^{+0.16}_{-0.88}) \times 10^{-7}$	1.023 ± 0.007

$\frac{d^2\sigma}{dp_T^{jet}dy^{jet}}$ $(1.1 < \lvert y^{jet}\rvert < 1.6)$		
p_T^{jet} [GeV/c]	$\sigma \pm$ (stat.) $\pm$ (sys.) [nb/(GeV/c)]	C_{HAD} parton $\rightarrow$ hadron
54 - 62	$(11.2 \pm 0.3^{+1.4}_{-1.4}) \times 10^{0}$	1.160 ± 0.125
62 - 72	$(4.48 \pm 0.15^{+0.72}_{-0.64}) \times 10^{0}$	1.133 ± 0.101
72 - 83	$(1.84 \pm 0.06^{+0.25}_{-0.24}) \times 10^{0}$	1.111 ± 0.081
83 - 96	$(7.31 \pm 0.37^{+0.98}_{-0.85}) \times 10^{-1}$	1.094 ± 0.065
96 - 110	$(3.02 \pm 0.05^{+0.41}_{-0.42}) \times 10^{-1}$	1.080 ± 0.052
110 - 127	$(1.15 \pm 0.03^{+0.17}_{-0.16}) \times 10^{-1}$	1.068 ± 0.042
127 - 146	$(4.14 \pm 0.04^{+0.69}_{-0.62}) \times 10^{-2}$	1.059 ± 0.034
146 - 169	$(1.41 \pm 0.02^{+0.26}_{-0.21}) \times 10^{-2}$	1.051 ± 0.027
169 - 195	$(4.22 \pm 0.04^{+0.90}_{-0.77}) \times 10^{-3}$	1.045 ± 0.021
195 - 224	$(1.16 \pm 0.02^{+0.30}_{-0.25}) \times 10^{-3}$	1.040 ± 0.016
224 - 259	$(2.76 \pm 0.09^{+0.87}_{-0.64}) \times 10^{-4}$	1.036 ± 0.012
259 - 298	$(5.22 \pm 0.23^{+1.83}_{-1.50}) \times 10^{-5}$	1.033 ± 0.009
298 - 344	$(8.13 \pm 0.62^{+5.22}_{-2.80}) \times 10^{-6}$	1.030 ± 0.006
344 - 396	$(1.05 \pm 0.22^{+0.43}_{-0.52}) \times 10^{-6}$	1.028 ± 0.003

$\frac{d^2\sigma}{dp_T^{jet}dy^{jet}}$ $(1.6 < \lvert y^{jet}\rvert < 2.1)$		
p_T^{jet} [GeV/c]	$\sigma \pm$ (stat.) $\pm$ (sys.) [nb/(GeV/c)]	C_{HAD} parton $\rightarrow$ hadron
54 - 62	$(6.89 \pm 0.16^{+1.05}_{-0.98}) \times 10^{0}$	1.132 ± 0.104
62 - 72	$(2.76 \pm 0.02^{+0.32}_{-0.31}) \times 10^{0}$	1.116 ± 0.087
72 - 83	$(1.07 \pm 0.01^{+0.14}_{-0.12}) \times 10^{0}$	1.100 ± 0.072
83 - 96	$(3.86 \pm 0.04^{+0.56}_{-0.51}) \times 10^{-1}$	1.086 ± 0.058
96 - 110	$(1.35 \pm 0.02^{+0.24}_{-0.19}) \times 10^{-1}$	1.072 ± 0.045
110 - 127	$(4.27 \pm 0.04^{+0.72}_{-0.62}) \times 10^{-2}$	1.059 ± 0.033
127 - 146	$(1.24 \pm 0.02^{+0.29}_{-0.23}) \times 10^{-2}$	1.047 ± 0.022
146 - 169	$(2.97 \pm 0.04^{+0.77}_{-0.60}) \times 10^{-3}$	1.035 ± 0.012
169 - 195	$(5.87 \pm 0.09^{+1.86}_{-1.40}) \times 10^{-4}$	1.024 ± 0.003
195 - 224	$(8.71 \pm 0.32^{+3.99}_{-2.70}) \times 10^{-5}$	1.013 ± 0.005
224 - 259	$(8.78 \pm 0.64^{+5.12}_{-3.10}) \times 10^{-6}$	1.003 ± 0.012
259 - 298	$(5.69 \pm 1.66^{+3.59}_{-3.30}) \times 10^{-7}$	0.993 ± 0.018

TABLE VI: Measured inclusive jet differential cross section as a function of p_T^{jet} for jets in the regions $0.7 < |y^{jet}| < 1.1$, $1.1 < |y^{jet}| < 1.6$, and $1.6 < |y^{jet}| < 2.1$. An additional 5.8% uncertainty on the luminosity is not included. The parton-to-hadron correction factors, $C_{HAD}(p_T^{jet})$, are applied to the pQCD predictions.